Epitaxial growth of alkali halides on stepped metal surfaces

A. Riemann,[1,2,*] S. Fölsch,[1,3] and K. H. Rieder[1]
[1]*Institut für Experimentalphysik, Freie Universität Berlin, D-14195 Berlin, Germany*
[2]*Department of Physics and Astronomy, University of British Columbia, Vancouver BC, Canada*
[3]*Paul-Drude-Institut für Festkörperelektronik, D-10117 Berlin, Germany*
(Received 26 April 2005; published 16 September 2005)

We present a growth study of the alkali halides NaCl and KCl on the stepped metal surfaces Cu(311) and Cu(221) using high resolution low energy electron diffraction. For all systems studied it was found that the alkali halide deposit forms (100)-terminated epitaxial layers which have essential structural features in common: The interfacial arrangement between the ionic adlayer and the stepped metal substrate is characterized by an alignment of the polar in-plane Cl ion rows parallel and perpendicular to the intrinsic Cu steps. For low coverages ($\sim$1 ML) the Cl ions are in registry with the intrinsic substrate steps causing uniaxial strain in the direction perpendicular to the steps. In contrast, parallel to the steps the Cl ions are free to adjust their optimum Cl-Cl spacing. For coverages $>$3 ML, the strain perpendicular to the intrinsic Cu steps is accommodated which suggests the incorporation of monoatomic Cu defect steps at the interface in this regime of higher coverage.

DOI: 10.1103/PhysRevB.72.125423 PACS number(s): 68.35.Bs, 61.14.Hg, 68.55.−a

I. INTRODUCTION

Insulating films are of general interest for technological applications as well as for a fundamental understanding in surface science. The availability of high-quality insulating layers represents an important aspect of technological use in order to realize for example resonant tunneling devices[1] and magnetic tunnel junctions.[2] Furthermore, due to their quasi-insulating behavior even in the thickness range of only a few monolayers (ML) such films provide a suitable template to partially decouple adsorbed organic molecules[3] or to study assembled metal and semiconductor nanostructures.[4] The growth of ultrathin insulating layers on conducting surfaces can be investigated by standard surface science methods since charging effects[5] do not hamper the measurement if the films are sufficiently thin and the substrate conductivity permits one to establish a stable electrostatic surface potential. Alkali halides (AH) represent the archetype ionic insulator material and provide a band gap in the range of 6.1 eV (CsI) to 13.6 eV (LiF) (Ref. 6) and a low chemical reactivity. In the case of semiconductor substrates, epitaxial AH growth has been achieved on various surfaces such as Ge(100),[7–9] Ge(111),[7,8] Si(100),[10] and GaAs(100).[10,11] With respect to metal surfaces work was reported on low-indexed substrates revealing the formation of films with rotation domain disorder on Cu(111),[12] textured layers on Al(100), and Al(111),[13] or step-induced directional alignment on Cu(100) (Ref. 14) and Ag(100).[14] A common feature of all these growth systems is that alkali halides preferably form (100)-terminated layers. This is reasonable since in bulk crystals it is the nonpolar (100) plane which is the only stable equilibrium crystal face due to the surface free energy minimization of this orientation.[15]

Contrasting these previous investigations of alkali halides on low-indexed metal substrates,[12–14] our recent work has shown that interfaces of exceptionally high stability are formed when ionic insulators such as alkali halides are grown on stepped metal surfaces of suitable orientation.[17–20] This enhanced interfacial stability is due to electrostatic interactions between the ionic charges of the overlayer and the charge modulation of the metal substrate surface. The charge modulation results from the redistribution of the electron cloud at a corrugated metal surface, as it was first discussed in the pioneering theoretical work of Smoluchowski in 1941.[16] Figure 1 shows a schematic cross section of the corrugated simple cubic (110) surface, where the bold lines mark the Wigner-Seitz cells of the first two atomic layers. To lower the kinetic energy $\sim[\nabla\rho(\vec{r})]^2$ of the electrons the charge distribution is smoothed out, which is depicted by the wavy line in the figure. The charge redistributes from the "hills" into the "valleys" formed by the surface atoms. In this way, a net positive charge arises on the "hills" and a negative charge in the "valleys" of the corrugated surface. Recent density functional theory (DFT) calculations by Olsson and Persson[21] have corroborated an appreciable role of electrostatic interactions in the binding between an ionic overlayer and a stepped metal surface along with covalent interactions which further enhance the binding.

In the present study, the criterion for enhanced interfacial stability (i.e., the geometric matching between the substrate steps and the spacing of adjacent polar ion rows along $\langle 110\rangle$) is verified for various AH/metal substrate combinations. Specifically, we explore the influence of film thickness on the interfacial structure and its interrelationship with the coverage-dependent evolution of epitaxial strain. For all investigated systems the same essential characteristics are

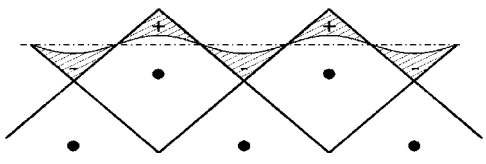

FIG. 1. Schematic charge distribution of a simple cubic (110) metal surface as described by Smoluchowski (Ref. 16). The zigzag line mimics the corrugation of the surface according to the bulk Wigner-Seitz cells; the wavy line represents the equilibrium charge distribution.

found: At low coverages (~1 ML) close-packed polar rows of ions are in perfect registry with the intrinsic substrate steps causing uniaxial strain in the direction perpendicular to the steps, while along the step direction the ion spacing is virtually free to adjust to its optimum value. For coverages >3 ML, the strain perpendicular to the intrinsic Cu steps is accommodated which suggests the incorporation of monoatomic Cu defect steps at the interface in this regime of higher coverage.

II. EXPERIMENT

The experiments for the present work were performed in an ultra-high vacuum (UHV) chamber equipped with a high resolution low energy electron diffraction (SPALEED=spot profile analyzing LEED) system[22] and various other tools for *in situ* sample preparation and characterization. All experiments were performed at a base pressure lower than 3×10^{-10} mbar. The samples were chemomechanically polished copper crystals in (311) and (221) orientation, respectively. The UHV sample preparation consisted of repeated Ne^+ sputtering cycles at energies between 900 and 1300 eV and currents of typically 5 μA. Subsequently to the sputtering, the samples were annealed at temperatures of 650 K for the Cu(311) crystal and 750 K for the Cu(221) crystal. The alkali halides NaCl and KCl [$a_{0,\mathrm{NaCl}}=5.64$ Å, $a_{0,\mathrm{KCl}}=6.29$ Å (Ref. 23)], both in powder form with 99.95% purity, were evaporated from Al_2O_3 crucibles at about 1000 K source temperature. Under these conditions, alkali halides sublimate in molecular form,[24] which preserves the stoichiometry of the deposited layers. The latter was confirmed *in situ* by x-ray photoelectron spectroscopy (XPS). The coverage of the alkali halide films was estimated by monitoring the XPS intensities representative for the Cu substrate (Cu $2p$) and the alkali halide film (Cl $2p$, Na $1s$, K $2p_{3/2}$), respectively.

The copper [$a_{0,\mathrm{Cu}}=3.61$ Å at 25 °C (Ref. 25)] substrate surface orientations used in this work correspond to Cu(311) and Cu(221). These surface orientations are vicinal to the (111) plane, i.e., they are regularly stepped surfaces with hexagonal close-packed (111) terraces. For the Cu(311) surface, these terraces are separated by intrinsic (100) steps. The close-packed rows at the edges of the intrinsic steps are at a distance of 4.23 Å. The primitive unit cell is represented by a parallelogram with side dimensions of 2.55 and 4.42 Å and an angle of 73.1° and 106.9° between the sides. A hard-sphere model of this surface is shown in Fig. 2(a) in side view along the steps (top) and in top view (bottom). The Cu(221) surface, on the other hand, consists of intrinsic (111) steps which are separated by 7.66 Å. The primitive unit cell of this vicinal surface is rectangular as can be seen in the corresponding top view hard-sphere model in Fig. 2(b) (bottom).

III. LEED RESULTS

Three different AH overlayer/substrate combinations were studied, namely, NaCl/Cu(311), KCl/Cu(311), and NaCl/Cu(221). In order to facilitate a clear comparison of

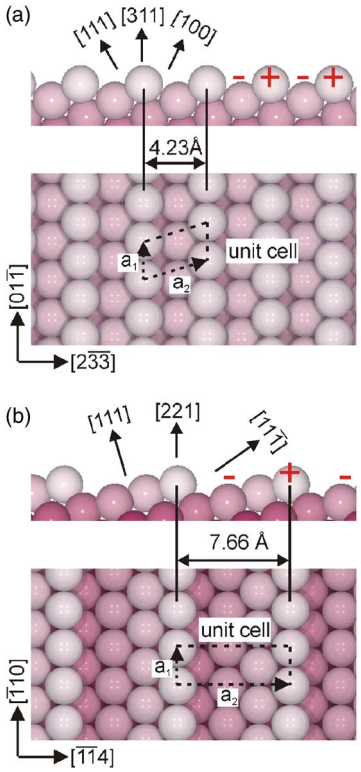

FIG. 2. (Color online) Hard-sphere models of (a) the Cu(311) surface and (b) the Cu(221) surface.

the inherent growth characteristics found, this section summarizes primary crystallographic features as extracted from high-resolution LEED measurements at different coverages. For each growth system, 1 to 6 ML were deposited at a rate of typically 0.25 to 1 ML per minute and at a substrate temperature of ~500 K followed by subsequent annealing at the same temperature for ten minutes. Prolonged annealing was applied in order to promote a resulting growth structure close to thermodynamic equilibrium.

The Cu(311) surface was prepared according to the procedure described above. As a result, a (1×1) LEED pattern with sharp and bright spots was observed, indicating a well-ordered bulk-terminated surface. From the halfwidth of the specular beam the average terrace size was estimated to correspond to ~290 Å along the $[\bar{2}\bar{3}\bar{3}]$ direction (perpendicular to the intrinsic Cu steps) and to ~410 Å along the $[01\bar{1}]$ direction (parallel to the intrinsic steps).

Figure 3(a) shows the LEED pattern observed after deposition of 1 ML NaCl. Here, the (1×1) Cu(311) unit cell is indicated by a dashed line together with the integral-order spots of the substrate surface. In addition, superstructure spots associated with the NaCl overlayer are present as indicated by fractional-order indices. It is convenient to express the oblique superstructure unit cell in matrix notation,[26] where the elements m_{ij} yield the real space superstructure unit vectors $\mathbf{b_1}$ and $\mathbf{b_2}$ as a function of the substrate unit vectors $\mathbf{a_1}$ and $\mathbf{a_2}$ according to $b_i=\Sigma_{j=1}^{2}m_{ij}a_j$. Accordingly, the epitaxial relationship between substrate and overlayer is expressed by a $\begin{pmatrix}3&0\\1&1\end{pmatrix}$ superstructure unit cell as indicated in Fig. 3(a) by a solid line. As a further prominent feature, a

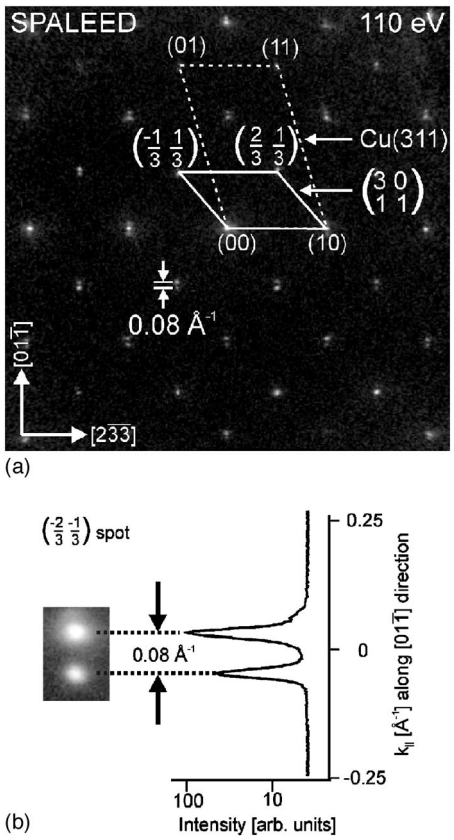

FIG. 3. LEED pattern and line scan of the $\left(-\frac{2}{3}-\frac{1}{3}\right)$ spot for 1 ML NaCl on Cu(311) deposited at 520 K. (a) Diffraction pattern with Cu(311) surface unit cell (dashed line) and NaCl adlayer-induced $\begin{pmatrix}3&0\\1&1\end{pmatrix}$ superstructure (full line); the superstructure spots (cf. fractional indices) are indexed with respect to the integral-order spot positions of the Cu(311) substrate. A spot splitting of 0.08 Å^{-1} in [01$\bar{1}$] direction, i.e., parallel to the intrinsic Cu steps is observed. (b) Profile of the $\left(-\frac{2}{3}-\frac{1}{3}\right)$ spot extracted from the diffraction pattern in (a) with the line scan taken parallel to the intrinsic Cu steps to analyze the spot splitting.

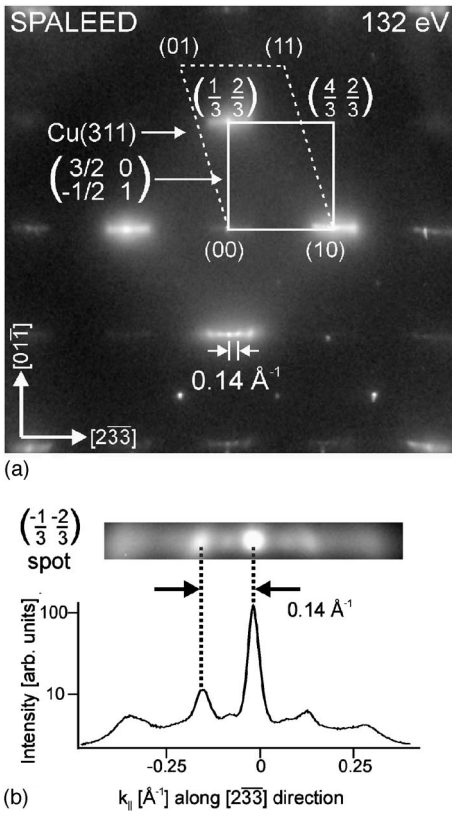

FIG. 4. LEED pattern and profile of the $\left(-\frac{1}{3}-\frac{2}{3}\right)$ spot for 6 ML NaCl on Cu(311) deposited at 520 K. (a) Diffraction pattern with the Cu(311) unit cell (dashed line) and the $\begin{pmatrix}3/2&0\\-1/2&1\end{pmatrix}$ superstructure (full line) which indicates bulk terminated NaCl(100) in $p(1\times1)$ configuration. A spot splitting of 0.14 Å^{-1} in the [2$\bar{3}$3] direction, i.e., perpendicular to the intrinsic steps of the template is observed. (b) Profile of the $\left(-\frac{1}{3}-\frac{2}{3}\right)$ spot taken from the diffraction pattern in (a) indicating the spot splitting in the direction perpendicular to the intrinsic Cu steps.

spot splitting of $\Delta k_{[01\bar{1}]}=0.08$ Å^{-1} along the [01$\bar{1}$] direction parallel to the intrinsic Cu steps is observed. The splitting is shown in more detail by the intensity profile of the $\left(-\frac{2}{3}\ -\frac{1}{3}\right)$ spot in Fig. 3(b). From the characteristic spot splitting a spatial correlation $2\pi/\Delta k_{[01\bar{1}]}=79$ Å along the intrinsic Cu step direction is derived, whose origin will be addressed in the next section. Figure 4(a) shows the LEED pattern for an increased coverage of 6 ML NaCl. In this stage the overlayer symmetry is described by a $\begin{pmatrix}3/2&0\\-1/2&1\end{pmatrix}$ superstructure unit cell (cf. solid line) which is essentially equivalent to a bulk-like (100) termination of the NaCl overlayer: For a perfect accommodation according to $\begin{pmatrix}3/2&0\\-1/2&1\end{pmatrix}$ symmetry the length of the orthogonal base vector is 1.64 and 1.48 Å^{-1} along [01$\bar{1}$] and [2$\bar{3}$3], respectively, while it is 1.58 Å^{-1} for bulk-terminated NaCl(100). As is also evident from the LEED pattern in Fig. 4(a), the splitting of superstructure spots along the Cu step direction has disappeared while a new spot splitting occurs perpendicular to the steps of the Cu substrate. The beam profile in Fig. 4(b) details a splitting of $\Delta k_{[2\bar{3}3]}=0.14$ Å^{-1} which is equivalent to a spatial correlation of 45 Å.

Next, we turn to the growth of KCl on the Cu(311) surface. As already noted above, the cubic bulk lattice constant of KCl is 10% larger compared to that of NaCl. The resulting epitaxial overlayer orientation can be inferred from the diffraction patterns in Fig. 5(a) after deposition of 1 ML KCl and in Fig. 6(a) after deposition of 6 ML KCl. For clarity, the Cu(311) primitive unit cell is again indicated in both LEED patterns by a dashed line. Figure 5(a) shows that the epitaxial accommodation of 1 ML KCl on Cu(311) leads to a different superstructure symmetry as compared to the case of NaCl monolayer growth on Cu(311) [cf. Fig. 3(a)]. Here, the superstructure is described by a $\begin{pmatrix}7&0\\3&1\end{pmatrix}$ unit cell, as denoted by a full line in Fig. 5(a). Again, however, a splitting of the superstructure spots is observed along the Cu step direction. In the present case, the splitting is $\Delta k_{[01\bar{1}]}=0.12$ Å^{-1} [see also the detailed profile in Fig. 5(b)] and corresponds to a real space correlation length of 52 Å, which is considerably smaller than that found for the NaCl monolayer on Cu(311). The LEED pattern obtained after depositing 6 ML KCl [cf. Fig. 6(a)] indicates overall structural features which are simi-

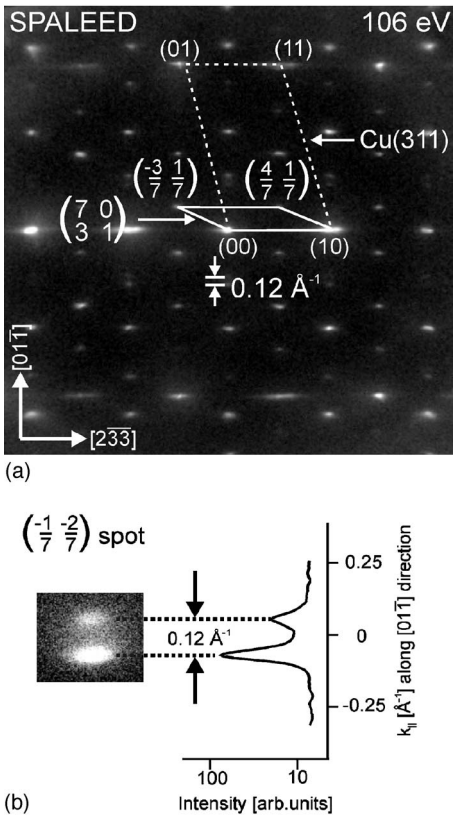

FIG. 5. LEED pattern and profile of the $\left(-\frac{1}{7}-\frac{2}{7}\right)$ spot for 1 ML KCl/Cu(311) deposited at 520 K. (a) Diffraction pattern with the Cu(311) unit cell (dashed line) and the KCl-induced $\binom{7\ 0}{3\ 1}$ superstructure cell (full line); a spot splitting is observed parallel to the intrinsic Cu steps along the $[01\bar{1}]$ direction. (b) Profile of the $\left(-\frac{1}{7}-\frac{2}{7}\right)$ spot parallel to the intrinsic Cu steps indicating a spot splitting of 0.12 Å^{-1}.

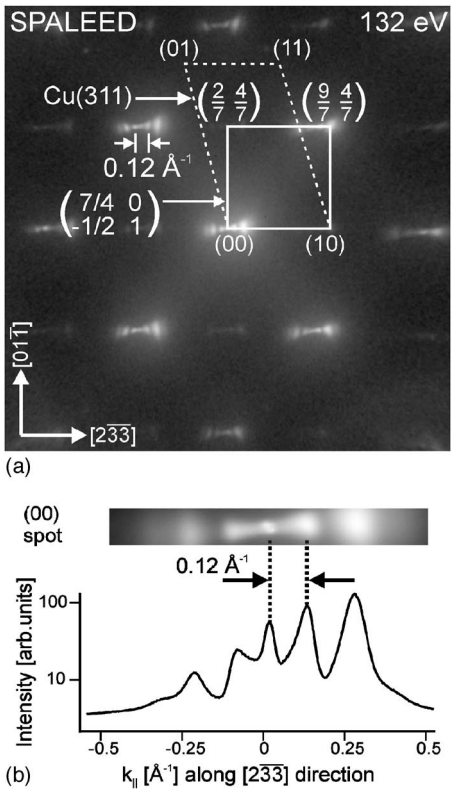

FIG. 6. LEED pattern and profile of the (00) spot for 6 ML KCl on Cu(311) deposited at 520 K. (a) In the diffraction pattern, the $\binom{7/4\ 0}{-1/2\ 1}$ superstructure induced by the KCl overlayer (full line) as well as the original Cu(311) unit cell (dashed line) are indicated; a spot splitting is observed perpendicular to the intrinsic Cu steps along the $[\bar{2}33]$ direction. (b) Profile of the specular (00) spot taken perpendicular to the intrinsic Cu steps, the spot splitting measures 0.12 Å^{-1} [the spot splitting indicated in LEED pattern is exemplary, the actual profile in (b) was taken at the specular (00) spot].

lar to the case of high-coverage NaCl growth on Cu(311) [cf. Fig. 4(a)]: The overlayer superstructure is described by a $\binom{7/4\ 0}{-1/2\ 1}$ unit cell close to that of bulk-terminated KCl(100). Again, a spot splitting perpendicular to the intrinsic steps of the Cu(311) template develops [see profile in Fig. 6(b)]. Here, the spot splitting measures $\Delta k_{[\bar{2}33]}=0.12$ Å^{-1}, which corresponds to a spatial correlation of ~52 Å perpendicular to the steps.

For the third AH overlayer/substrate combination studied, the Cu(221) surface was chosen to provide a template with a considerably larger step spacing as compared to the Cu(311) surface [7.66 Å for Cu(221) compared to 4.23 Å for Cu(311)]. After repeated preparation cycles, a sharp (1×1) diffraction pattern with a rectangular unit cell was observed in accordance with the surface symmetry of Cu(221) as shown in the sphere model in Fig. 2(b). The average terrace width was estimated to be ~70 Å along the $[\bar{1}14]$ direction, which is perpendicular to the intrinsic Cu steps, and ~85 Å along the $[\bar{1}10]$ direction, i.e., parallel to the intrinsic steps. The resulting diffraction pattern for 1 ML NaCl coverage is shown in Fig. 7(a) and verifies that the superstructure of the overlayer can be expressed in conventional notation corresponding to a (1×3) unit cell (cf. full line); the primitive unit cell of the substrate is denoted by a dashed line. In line with the previous two cases of low-coverage growth, the superstructure spots are split up along the Cu step direction as indicated in Fig. 7(b). This characteristic splitting $\Delta k_{[\bar{1}10]}=0.11$ Å^{-1} corresponds to a real space correlation of 57 Å. Finally, at 6 ML NaCl coverage the overlayer periodicity transforms into a $(3/2\times1/2)$ superstructure [see full line in Fig. 8(a)] which again is consistent with a (100) bulk termination prevailing at higher coverage. The spot splitting of $\Delta k_{[\bar{1}\bar{1}4]}=0.10$ Å^{-1} observed in this high-coverage regime [cf. spot profile in Fig. 8(b)] indicates a spatial correlation 63 Å perpendicular to the intrinsic Cu steps.

IV. DISCUSSION

A. Low alkali halide coverage

Our diffraction data show that the alkali halides NaCl and KCl form (100)-terminated epitaxial layers on both the Cu(311) and the Cu(211) surface. This observation reflects the outcome of previous calculations of the surface energies of different crystallographic orientations[27,28] and the equilibrium shape of the bulk crystal,[15] which identified the (100)

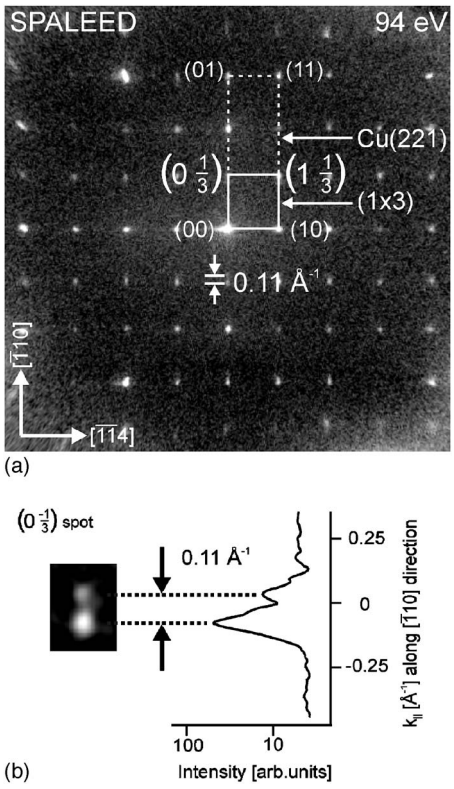

FIG. 7. LEED pattern and profile of the $(0\,-\frac{1}{3})$ spot for 1 ML NaCl on Cu(221) deposited at 470 K. (a) Diffraction pattern with the primitive Cu(221) unit cell (dashed line) and the (1×3) superstructure cell (full line); (b) $(0\,-\frac{1}{3})$ spot profile measured parallel to the intrinsic Cu step direction indicating a spot splitting of 0.11 $Å^{-1}$.

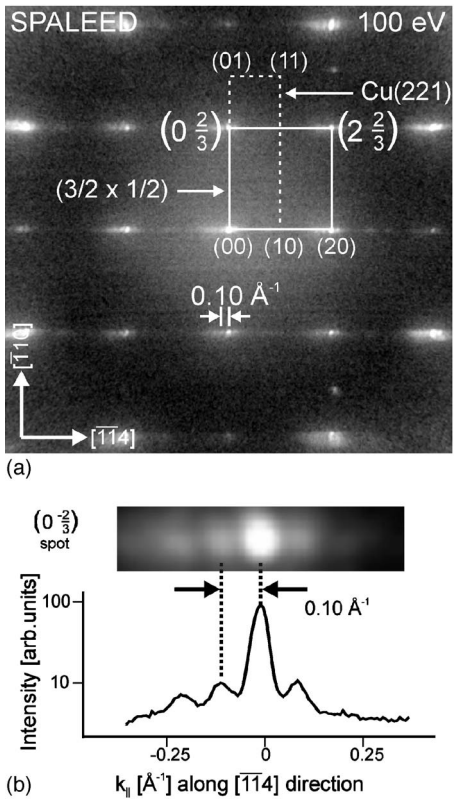

FIG. 8. LEED pattern and profile of the $(0\,-\frac{2}{3})$ spot for 6 ML NaCl on Cu(221) deposited at 470 K. (a) Diffraction pattern with $(3/2\times1/2)$ NaCl-induced superstructure (full line) indicative for bulk-terminated NaCl(100) in $p(1\times1)$ configuration and with the original Cu(221) unit cell (dashed line). (b) $(0\,-\frac{2}{3})$ spot profile measured perpendicular to the intrinsic Cu steps showing a spot splitting of 0.10 $Å^{-1}$.

planes as the only stable equilibrium planes for NaCl and other fcc alkali halides. Likewise, exclusively (100)-terminated layers are found for alkali halide growth on various semiconductor and metal substrates[7,9,10,12–14] [with the exception of nonstochiometric ultrathin NaCl(111) islands formed by subsequent Na and Cl_2 adsorption on Al(100) and Al(111) (Ref. 29)]. The overlayer structures derived from the present LEED data verify epitaxial registry between the film and the stepped metal substrate. For all three investigated AH/substrate combinations we find that the polar $\langle 110\rangle$ in-plane directions of the adlayer, which span the sides of the $p(1\times1)$ alkali halide unit cell, run parallel and perpendicular to the intrinsic Cu step direction; this is in line with the azimuthal film orientation which we have previously observed for the growth systems KCl/Cu(211) and RbI/Cu(211).[30]

Based on a series of scanning tunneling microscopy (STM) experiments on NaCl/Cu(311) monolayer films[18] we have found that rows of identical ions parallel to the step direction are in strict registry with the Cu step periodicity with the Cl ions located on top of the step edges and the Na ions between the steps. This specific ordering behavior was attributed to the charge corrugation of the stepped surface due to the Smoluchowski effect[16] of lateral electron charge smoothing. Recently, Olsson and Persson[21] verified this assignment by DFT calculations showing that the adsorption energy of a (100)-terminated NaCl monolayer with the Cl ions located on top of the Cu step edges is significantly higher than in the case of (i) an in-plane alignment with the Na ions located on top of the steps or (ii) a NaCl monolayer adsorbed on a less corrugated surface [such as NaCl/Cu(100)]. Furthermore, the DFT calculations show that a directed covalent interaction exists between the Cl ions and the Cu atoms at the step edges deriving from the interaction between Cl $3p$ states and Cu d states. On the basis of these findings, the alkali halide overlayer configurations obtained from the LEED data will be analyzed in the following.

The adsorption configuration of the NaCl/Cu(311) monolayer with Cl ions located on top of the Cu steps is visualized in side view in the upper part of Fig. 9. This interfacial geometry imposes a Cl-Cl spacing of 4.23 Å along the $[2\bar{3}3]$ direction, i.e., perpendicular to the Cu steps. In the center panel, the $\binom{3\ 0}{1\ 1}$ superstructure of the NaCl film [cf. Fig. 3(a)] with respect to the underlying Cu(311) template is illustrated. Regarding the position of the Cl ions parallel to the intrinsic steps, two different $\binom{3\ 0}{1\ 1}$ configurations are possible. The center and lower panel of the hard-sphere model in Fig. 9 show, respectively, these configurations of the NaCl adlayer. In the first configuration the Cl ions alternate in on-top and bridge positions along the Cu step edges. In the second configura-

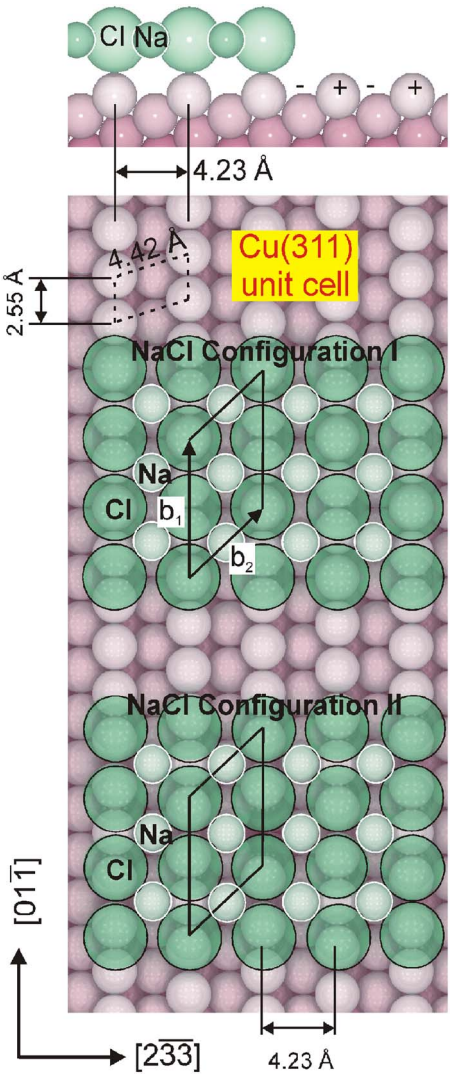

FIG. 9. (Color online) Hard-sphere model of the Cu(311) surface with 1 ML NaCl. Top: Side view of the Cu(311) surface with indicated charge modulation, the Cl ions are on top of intrinsic steps; middle: NaCl configuration I with the Cl ions in alternating on-top and bridge positions atop of the close-packed Cu rows; bottom: NaCl in configuration II, the Cl ions are shifted by $\frac{1}{4}$ of a Cu-Cu spacing along the intrinsic Cu steps with respect to configuration I; both configurations exhibit $\binom{3\ 0}{1\ 1}$ overlayer symmetry with respect to the Cu(311) surface.

tion, the NaCl film is shifted along the steps by $\frac{1}{4}$ of a Cu-Cu distance with respect to the first configuration. As a result, all Cl ions are in equivalent positions with respect to the underlying template, but the Na ions in the troughs between the steps are in alternating positions, which results in the $\binom{3\ 0}{1\ 1}$ configuration of this second arrangement. DFT calculations[21] indicate that the adsorption energies for these two configurations are almost degenerate, which indicates that both structures should coexist on the surface. Furthermore, the energy cost for stretching an isolated monolayer to match the (311) surface lattice is only 0.063 eV per Na-Cl pair, and site-dependent NaCl-Cu interactions are sufficient for a commensurate growth of the monolayer. STM studies of a monomolecular NaCl layer on Cu(311) (Refs. 18, 20, and 31) reveal that the two configurations indeed coexist. In Refs. 18 and 20 we referred to these configurations as the $c(2\times2)$ structure (configuration I in Fig. 9) and the $p(1\times1)$ structure (configuration II) with respect to the bulk-terminated unit cell of NaCl(100). Since STM detects only the Cl ions imaged as protrusions[13] configuration I leads to a corrugation characterized by $c(2\times2)$ symmetry (Cl ions occupy alternating adsorption sites) while configuration II shows $p(1\times1)$ symmetry (Cl ions are on equivalent sites). The two different configurations occur in a periodic structure of alternating domains along the Cu step direction, where equivalent adjacent domains are shifted by half a $c(2\times2)$ unit cell. This corresponds to a shift of half a Cu-Cu distance of the Cl ions with respect to the underlying template. This antiphase domain disorder[32] leads to the spot splitting of 0.08 $Å^{-1}$ observed in the LEED pattern in Fig. 3. The corresponding periodic length is $L=79$ Å in real space, with L as the mean separation of equivalent domains. Regarding the two commensurate $c(2\times2)$ configurations shown in the hard-sphere model, the spacing $a_{\mathrm{NaCl},\|}$ between two Cl ions along the intrinsic steps would be $3.82\ Å=1.5\times2.55$ Å (Cu-Cu spacing $a_{\mathrm{Cu},\|}=2.55$ Å). Due to the alternating domain structure with a shift of half a Cu-Cu spacing between adjacent domains, however, the average Cl-Cl spacing is actually $a_{\mathrm{NaCl},\|}=1.5a_{\mathrm{Cu},\|}[1\pm(a_{\mathrm{Cu},\|}/2/L)]$. For an expansion of the adlayer with respect to the perfectly commensurate structure (corresponding to a plus sign in the equation) the Cl-Cl spacing is 3.89 Å, whereas a contraction (corresponding to a minus sign) would lead to a Cl-Cl spacing of 3.77 Å. The lattice constant of the isolated monolayer was calculated to be 5.55 Å,[21] which results in a Cl-Cl distance of 3.92 Å. If the adlayer expands in the described way the strain along the intrinsic Cu steps is reduced to less than -1%.

The detailed positioning of a 1-ML-thick NaCl film relative to the Cu(311) substrate can be summarized as follows: Perpendicular to the Cu steps, the Cl ions are localized at the step positions and the Cl-Cl distance along this direction is given by the step spacing of 4.23 Å, leading to a tensile strain of about 8%. Parallel to the steps, on the other hand, the Cl ions are less localized and the average Cl-Cl distance along this direction is close to the fully relaxed value (corresponding to 3.92 Å calculated for the freestanding monolayer[21]).

For the case of 1 ML KCl on Cu(311) equivalent adlayer configurations are found: The Cl ions are on top of the intrinsic Cu steps and the K ions are in the troughs between the steps which leads to compressive strain perpendicular to the Cu steps. The position of the Cl ions parallel to the intrinsic steps can be determined from the LEED pattern in Fig. 5(a) with the corresponding hard-sphere model in Fig. 10. The KCl overlayer is characterized by a $\binom{7\ 0}{3\ 1}$ superstructure with respect to the underlying Cu(311) substrate. A locally commensurate layer is achieved if four Cl-Cl spacings match with seven Cu-Cu spacings along the [01$\bar{1}$] direction. The Cl-Cl distance for this commensurate arrangement is 4.47 Å parallel to the intrinsic steps. Similar to the system NaCl/Cu(311), a spot splitting in this direction is observed, which suggests that a periodic structure with alternating domains along the step direction forms also in the present case.

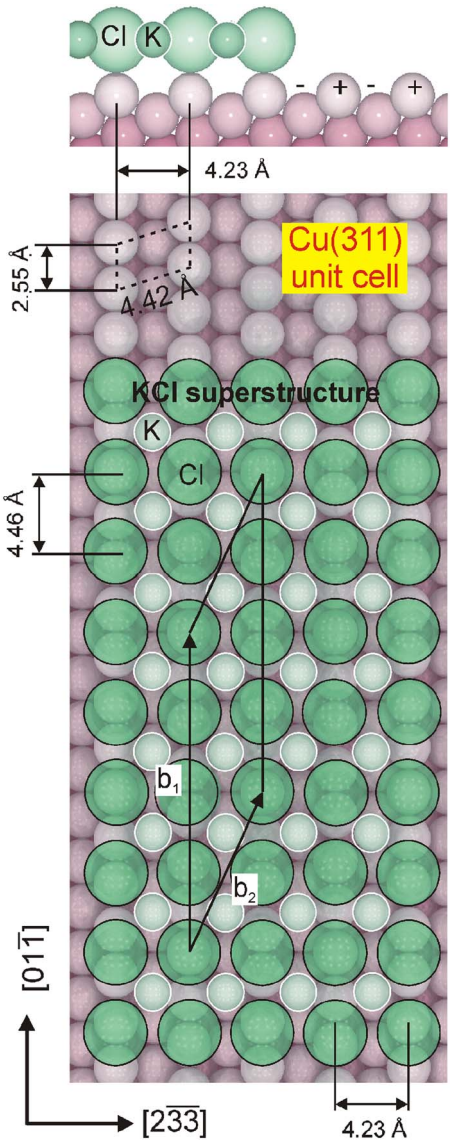

FIG. 10. (Color online) Hard-sphere model of the Cu(311) surface with 1 ML KCl. Top: Side view of the adlayer configuration with the Cl ions on top of the intrinsic Cu steps and the K ions in the troughs between the steps; bottom: Locally commensurate KCl $\begin{pmatrix} 7 & 0 \\ 3 & 1 \end{pmatrix}$ configuration with 4 Cl-Cl spacings matching 7 Cu-Cu spacings along the $[01\bar{1}]$ Cu step direction, the rhombic KCl unit cell is also indicated.

The separation of equivalent domains can be calculated from the spot splitting of 0.12 $Å^{-1}$ and corresponds to $L=52$ Å. Due to the size of the KCl superstructure unit cell the shift between two adjacent domains would be $\frac{1}{4}$ of a Cu-Cu spacing and the resulting Cl-Cl spacing would be $a_{\mathrm{KCl},\parallel} = \frac{1}{4} \times 7 \times a_{\mathrm{Cu},\parallel}[1 \pm (a_{\mathrm{Cu},\parallel}/4/L)]$. An expansion with respect to the perfectly commensurate matching of the adlayer along the steps leads to a Cl-Cl spacing of 4.52 Å, while a contraction would result in a Cl-Cl spacing of 4.41 Å. Although there are no calculations on isolated monolayers of KCl reported in the literature, it can be assumed to a first approximation [in analogy to the case of NaCl (Ref. 21)] that the lattice constant for an isolated monolayer is also in this case about 1.5% smaller than the bulk value (6.20 Å versus 6.29 Å) resulting in a Cl-Cl distance of 4.38 Å. A contraction of the KCl adlayer in the described way leads subsequently to a strain of less than 1% in the direction parallel to the intrinsic Cu steps.

For the system NaCl/Cu(221) the spacing of the intrinsic Cu steps measures 7.66 Å; thus, it is so large that only every other Cl row along the $[\bar{1}14]$ direction is positioned on top of the intrinsic steps. This leads to a Cl-Cl spacing of 3.83 Å and a compressive strain of −3% along this direction. From the LEED pattern in Fig. 7(a) it is evident that the NaCl adlayer adopts (1×3) symmetry with respect to the Cu(221) template. This configuration corresponds to a $p(2 \times 2)$ structure with respect to the $p(1 \times 1)$ symmetry of bulk-terminated NaCl(100). Similar to the case of 1 ML NaCl on Cu(311), this configuration leads to alternating domains of (1×3) symmetry along the direction parallel to the steps (cf. hard-sphere model in Fig. 11) with the Cl ions either in on top and bridge position or shifted by $\frac{1}{4}$ Cu-Cu distance. Again, the separation of equivalent domains can be obtained from the spot splitting of 0.11 $Å^{-1}$ which corresponds to $L=57$ Å in real space. For the expansion case a Cl-Cl distance of 3.91 Å is obtained, whereas a contraction with respect to the perfectly commensurate configuration leads to a Cl-Cl distance of 3.74 Å. The first case matches the calculated monolayer Cl-Cl spacing (3.92 Å) almost perfectly.

B. Higher alkali halide coverage

For alkali halide coverages of about 6 ML, the observed overlayer structures of the three investigated systems described by $\begin{pmatrix} 3/2 & 0 \\ -1/2 & 1 \end{pmatrix}$ symmetry for NaCl/Cu(311) [cf. Fig. 4(a)], $\begin{pmatrix} 7/4 & 0 \\ -1/2 & 1 \end{pmatrix}$ symmetry for KCl/Cu(311) [cf. Fig. 6(a)], and $(3/2 \times 1/2)$ symmetry for NaCl/Cu(221) [cf. Fig. 8(a)], are equivalent to the $p(1 \times 1)$ structure indicative for bulk-terminated alkali halide in (100) orientation. Only the spots indicative for this configuration prevail in the LEED patterns of the three systems. The spots connected with the different superstructure configurations in the low coverage regime, which are caused by the interfacial adjustment of the alkali halide adlayer with respect to the substrate are not apparent anymore because the LEED pattern is exclusively determined by diffraction involving the topmost atomic layers of the 6-ML-thick film. Nevertheless, a prominent feature is apparent from the spot profiles: A splitting perpendicular to the intrinsic step direction is observed; the respective spot profiles are shown in Figs. 4(b), 6(b), and 8(b) (note that in the low-coverage cases the spot splitting is parallel to the intrinsic Cu steps). The splitting reveals a superimposed periodicity perpendicular to the Cu step direction with a characteristic length of $2\pi/\Delta k$ (Δk is the measured spot splitting) which may originate from the formation of a regular defect structure formed at the film/substrate interface or a long-range corrugation (Moiré pattern) of the adlayer. Supplementary STM investigations at about 4 ML NaCl coverage on Cu(311) (Ref. 33) at an elevated growth temperature of 450 K favor the interpretation that substrate defect steps are formed at the interface since the experimental observations

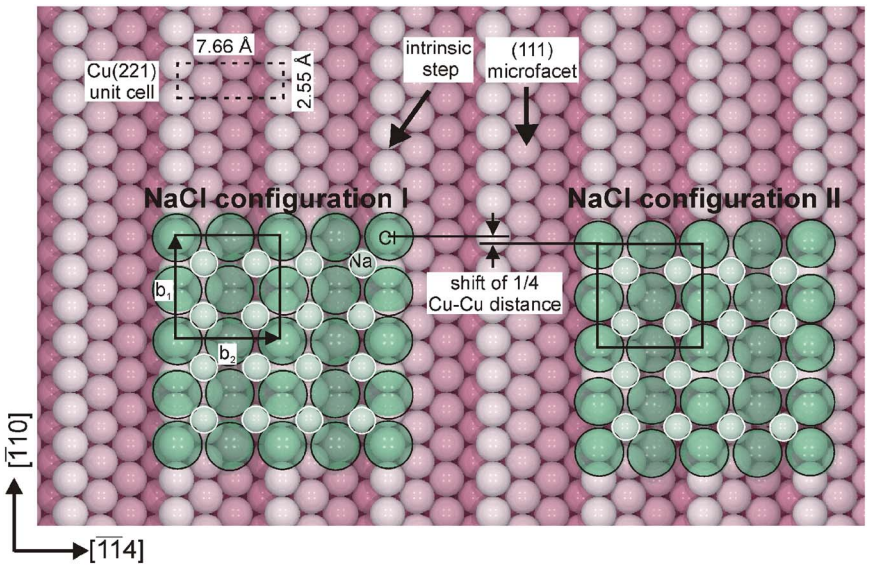

FIG. 11. (Color online) Hard-sphere model of the Cu(221) surface with 1 ML NaCl; the (1×3) overlayer structure with respect to the Cu(221) geometry is equivalent to $p(2\times2)$ structure of the NaCl(100) film with respect to the bulk-terminated $p(1\times1)$ configuration; left: NaCl in the first $p(2\times2)$ configuration, Cl ion rows running parallel to the intrinsic steps are located on top of the steps and in the middle of the (111) microfacets of the Cu(221) surface; the Cl ions atop of the Cu steps are in alternating on-top and bridge positions; right: NaCl in the second $p(2\times2)$ configuration which is shifted by $\frac{1}{4}$ of a Cu-Cu spacing along to the step direction with respect to the first $p(2\times2)$ configuration.

give no indication for the formation of Moiré pattern structures. Instead, a scenario of regularly separated defect steps overgrown by NaCl in the so-called carpet mode[34] appears more conclusive to explain the present interface structure. We have found a similar process of defect step formation upon NaCl growth on the kinked surface Cu(532):[17,31] In that case, STM measurements revealed the formation of monatomic defect steps at the interface between a kinked (531)-oriented facet and a (100)-terminated NaCl monolayer allowing for effective strain relaxation in the overlayer. Clearly, stress in heteroepitaxial growth increases with the film thickness. To accommodate this stress, the formation of misfit dislocations by means of regular steps in the substrate is a well-known mechanism.[35] Although the LEED images are not conclusive about the origin of the spot splitting, from the previous examples we prefer the hypothesis of the formation of defect steps to relieve uniaxial stress perpendicular to the intrinsic Cu steps instead of a large-range corrugation of the adlayer.

From the spot splitting of 0.14 $Å^{-1}$ in the case of 6 ML NaCl on Cu(311) [cf. Fig. 4(b)], a separation of ~45 Å is deduced for the monatomic defect steps which run parallel to the intrinsic steps. The following consideration illustrates that the present defect step array mediates an effective stress relaxation in the NaCl film. The defect step periodicity equals the distance of ten spacings between the intrinsic Cu steps plus the lateral shift connected with a monatomic defect step in the substrate. The adlayer consists of eleven NaCl units along this direction to match the defect step periodicity in a commensurate manner, which results in an average Cl-Cl spacing of 4.05 Å

$$10\times4.23\ \text{Å}+2.31\ \text{Å (lateral shift)}$$
$$=44.6\ \text{Å}=11\ \text{(NaCl units)}$$
$$\times4.05\ \text{Å}\ (a_{0,\text{NaCl}}/\sqrt{2}=3.99\ \text{Å}).$$

This interfacial matching is illustrated by the hard-sphere model in Fig. 12. The model shows the stepped structure of the Cu(311) surface along the $[2\bar{3}3]$ direction, i.e., perpendicular to the intrinsic steps. For clarity, only one NaCl monolayer is drawn and only the Cl ions are shown. The model shows that the incorporation of periodic steps largely reduces the initial tensile strain while keeping the Cl ions close to the step positions.

For the other two systems, equivalent matching conditions are found. For the case of 6 ML KCl on Cu(311), the spot splitting is 0.12 $Å^{-1}$ [cf. spot profile in Fig. 6(b)] which corresponds to ~52 Å. This distance represents 12 spacings between the intrinsic steps plus the lateral shift for the defect step. Here, the adlayer consists of 12 KCl unit cells which changes the effective average Cl-Cl spacing to 4.42 Å

$$12\times4.23\ \text{Å}+2.31\ \text{Å (lateral shift)}$$
$$=53.1\ \text{Å}=12\ \text{(KCl units)}$$
$$\times4.42\ \text{Å}\ (a_{0,\text{KCl}}/\sqrt{2}=4.45\ \text{Å}).$$

The initial compressive strain perpendicular to the steps is mostly reduced by the incorporation of the defect steps.

In the case of 6 ML NaCl on Cu(221), the LEED pattern and the spot profile in Fig. 8 show a spot splitting of 0.10 $Å^{-1}$ equivalent to a spatial correlation length of ~63 Å. This corresponds to eight intrinsic step spacings plus the

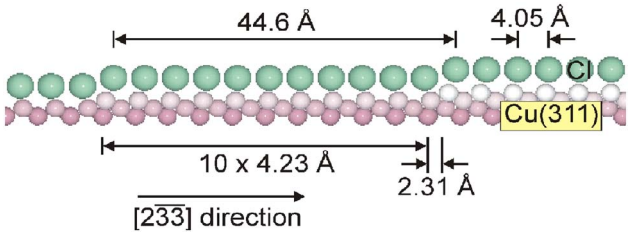

FIG. 12. (Color online) Hard-sphere model illustrating the NaCl-induced Cu defect step formation at the NaCl/Cu(311) interface as observed for 6 ML NaCl on Cu(311). For clarity, only one monolayer NaCl and only the Cl ions are shown in the scheme. Monatomic Cu defect steps are incorporated after every ten intrinsic step spacings.

lateral shift due to the defect step matching 16 NaCl units with a Cl-Cl spacing of 3.96 Å

$$8 \times 7.66\ \text{Å} + 2.13\ \text{Å (lateral shift)}$$
$$= 63.4\ \text{Å} = 16\ \text{(NaCl units)}$$
$$\times 3.96\ \text{Å}\ (a_{0,\text{NaCl}}/\sqrt{2} = 3.99\ \text{Å}).$$

The NaCl film is almost completely strain free with respect to the bulk lattice value perpendicular to the intrinsic steps.

V. SUMMARY

The present growth study of the alkali halides NaCl and KCl on stepped Cu surfaces shows together with our previous work on related AH/metal substrate combinations[18,30] that this class of growth systems is governed primarily by two general facts: (i) The nonpolar (100) termination is energetically highly favorable for fcc-type alkali halides, and (ii) corrugated metal surfaces are characterized by a surface charge modulation due to the Smoluchowski smoothing effect.[16] Enhanced interfacial stability is achieved when the interface geometry allows for a matching between the adlayer ions and the charge modulation of the corrugated metal surface. In the case of a stepped surface, the charge smoothing produces stripes of positive charge along the step positions and stripes of negative charge between the steps. Enhanced stability and thereby epitaxial layer growth is thus achieved when the step spacing matches with the spacing of polar ion rows in the (100) film plane (given by the nearest-neighbor spacing of identical ions along ⟨110⟩). Epitaxially strained layers of NaCl on Cu(311), KCl on Cu(311), and NaCl on Cu(221) as studied here obey this criterion, thus showing an alignment of the polar in-plane directions parallel and perpendicular to the intrinsic Cu steps with the Cl ions located on top of the steps.

The coverage-dependent evolution and accommodation of epitaxial strain was investigated in detail revealing general features which all growth systems studied have in common: In the monolayer regime, the rows of Cl ions are in strict registry with the intrinsic steps. Along the steps, however, the Cl ions are basically free to adopt an average Cl-Cl spacing close to the fully relaxed value which leads to the formation of antiphase domains along this direction. Hence, the AH monolayer is under uniaxial strain perpendicular to the Cu steps. With increasing coverages this strain is relieved by the incorporation of monatomic defect steps at the AH layer/substrate interface. In this way, the uniaxial stress connected with the heteroepitaxial growth of the alkali halide film on the stepped metal substrate is accommodated at higher film thickness. By means of STM we have previously observed a similar process of defect step incorporation also for the kinked template Cu(531) overgrown by a NaCl monolayer.[17]

Finally, it is noted that the present interface stabilization can also lead to massive surface faceting if (i) a facet orientation fulfilling the stability criterion is available close to the macroscopic substrate surface orientation and if (ii) sufficient adatom mobility allows for the required mass transport. Such faceting processes have been observed for the systems NaCl/Cu(211),[19,20] KCl/Ag(211),[31] and NaCl/Cu(532) (Ref. 17) and can be fully understood on the basis of geometric matching conditions as described above. The growth of alkali halides on vicinal metal surfaces can thus be exploited either to grow ultrathin epitaxial insulator films or to produce nanoscopic surface patterns by means of adsorbate-induced faceting and selective growth.

ACKNOWLEDGMENTS

This work was supported by the Volkswagen-Stiftung (I/72 417) and the Deutsche Forschungsgemeinschaft (RI 472/3-2, Sfb 290/TPA5).

*Corresponding author. Present address: Department of Physics and Astronomy, University of British Columbia, Vancouver, BC V6T1Z1. Email address: ariemann@physics.ubc.ca

[1] M. Watanabe, T. Suemasu, S. Muratake, and M. Asada, Appl. Phys. Lett. **62**, 300 (1993).
[2] W. Zhu, C. J. Hirschmugl, A. D. Laine, B. Sinkovic, and S. S. P. Parkin, Appl. Phys. Lett. **78**, 3103 (2001).
[3] J. Repp, G. Meyer, S. M. Stojković, A. Gourdon, and C. Joachim, Phys. Rev. Lett. **94**, 026803 (2005).
[4] T. Yamada, J. Vac. Sci. Technol. A **17**, 1463 (1999).
[5] P. S. P. Wei, Surf. Sci. **24**, 219 (1971).
[6] R. T. Poole, J. G. Jenkin, J. Liesegang, and R. C. G. Leckey, Phys. Rev. B **11**, 5179 (1975).
[7] S. Fölsch, U. Barjenbruch, and M. Henzler, Thin Solid Films **172**, 123 (1989).
[8] C. Schwennicke, J. Schimmelpfenning, and H. Pfnür, Surf. Sci. **293**, 57 (1993).
[9] D. A. Lapiano-Smith, E. A. Eklund, F. J. Himpsel, and L. J. Terminello, Appl. Phys. Lett. **59**, 2174 (1991).
[10] K. Saiki, Y. Nakamura, N. Nishida, W. Gao, and A. Koma, Surf. Sci. **301**, 29 (1994).
[11] K. Saiki, Y. Nakamura, and A. Koma, Surf. Sci. **269/270**, 790 (1992).
[12] R. Bennewitz, V. Barwich, M. Bammerlin, C. Loppacher, M. Guggisberg, A. Baratoff, E. Meyer, and H. J. Güntherodt, Surf. Sci. **438**, 289 (1999).
[13] W. Hebenstreit, J. Redinger, Z. Horozova, M. Schmid, R. Podloucky, and P. Varga, Surf. Sci. **424**, L321 (1999).
[14] M. Kiguchi, S. Entani, K. Saiki, H. Inoue, and A. Koma, Phys. Rev. B **66**, 155424 (2002).
[15] A. C. Shi and M. Wortis, Phys. Rev. B **37**, 7793 (1988).
[16] R. Smoluchowski, Phys. Rev. **60**, 661 (1941).
[17] S. Fölsch, A. Riemann, J. Repp, G. Meyer, and K. H. Rieder, Phys. Rev. B **66**, 161409(R) (2002).
[18] J. Repp, S. Fölsch, G. Meyer, and K. H. Rieder, Phys. Rev. Lett. **86**, 252 (2001).
[19] S. Fölsch, A. Helms, S. Zöphel, J. Repp, G. Meyer, and K. H. Rieder, Phys. Rev. Lett. **84**, 123 (2000).

[20] S. Fölsch, A. Helms, A. Riemann, J. Repp, G. Meyer, and K. H. Rieder, Surf. Sci. **497**, 113 (2002).
[21] F. Olsson and M. Persson, Surf. Sci. **540**, 172 (2003).
[22] U. Scheithauer, G. Meyer, and M. Henzler, Surf. Sci. **178**, 441 (1986).
[23] R. W. G. Wyckoff, *Crystal Structures* (Interscience, New York, 1965).
[24] G. M. Rothberg, M. Eisenstadt, and P. Kusch, J. Chem. Phys. **30**, 517 (1959).
[25] W. B. Pearson, *A Handbook of Lattice Spacing and Structure of Metals and Alloys* (Pergamon Press, New York, 1958).
[26] G. Ertl and J. Küppers, *Low Energy Electrons and Surface Chemistry* (VCH Verlagsgesellschaft, Weinheim, 1985).
[27] G. C. Benson, J. Chem. Phys. **35**, 2113 (1961).
[28] D. Wolf, Phys. Rev. Lett. **68**, 3315 (1992).
[29] W. Hebenstreit, M. Schmid, J. Redinger, R. Podloucky, and P. Varga, Phys. Rev. Lett. **85**, 5376 (2000).
[30] S. Fölsch, A. Helms, and K. H. Rieder, Appl. Surf. Sci. **162–163**, 270 (2000).
[31] A. Riemann, Ph.D. thesis, Freie Universität Berlin (2002).
[32] M. Henzler, in *Electron Spectroscopy for Surface Analysis*, edited by H. Ibach (Springer-Verlag, Berlin, 1977).
[33] J. Repp (private communication).
[34] J. Repp, Master's thesis, Freie Universität Berlin (1999).
[35] J. W. Matthews, in *Physics of Thin Films*, edited by G. Hass and R. E. Thun (Academic Press, New York, 1967), Vol. 4.